Extension of the reactor dynamics code DYN3D to SFR applications – Part II: validation against the Phenix EOL control rod withdrawal tests

Nikitin, E.; Fridman, E.;

Originally published:

May 2018

Annals of Nuclear Energy 119(2018), 411-418

DOI: https://doi.org/10.1016/j.anucene.2018.05.016

Perma-Link to Publication Repository of HZDR:

https://www.hzdr.de/publications/Publ-27089

Extension of the reactor dynamics code DYN3D for SFR applications – Part II: validation against the Phenix EOL control rod withdrawal tests

E. Nikitin [a,b,*], E. Fridman [a], and A. Pautz [b]

[a] *Helmholtz-Zentrum Dresden-Rossendorf, Bautzner Landstraße 400, 01328 Dresden, Germany*

[b] *Ecole Polytechnique Fédérale de Lausanne, CH-1015 Lausanne, Switzerland*

Keywords:

SFR, Phenix EOL tests, thermal expansion, nodal diffusion, transient analysis, DYN3D, Serpent

Abstract

The reactor dynamics code DYN3D, initially developed for LWR applications, is being extended for steady state and transient analyses of Sodium cooled Fast Reactor (SFR) cores. The extension includes the development of the few-group cross section generation methodology, updating of the thermal-hydraulic database with thermal-physical properties of sodium, and development of the thermal-mechanical model to account for thermal expansion effects of the core components.

Part I of the paper provided a detailed description of the recently implemented thermal expansion models able to treat axial expansion of fuel rod and radial expansion of diagrid. The results of the initial verification test were also presented in Part I of the paper.

The capability of the extended version of DYN3D to perform steady state and transient analyses of SFR cores was validated using selected tests from the end-of-life experiments conducted at the Phenix reactor. Part II of the paper reports on the results of the steady state analysis of the control rod withdrawal tests from the Phenix end-of-life experiments. The transient analysis of the initial stage of the natural circulation test is covered in Part III of the paper.

* Corresponding author: e.nikitin@hzdr.de

1. Introduction

The reactor dynamics code DYN3D (Rohde et al., 2016), initially developed for LWR applications, is being extended for steady-state and transient analyses of Sodium cooled Fast Reactor (SFR) cores. The extension includes the development of the few-group cross section (XS) generation methodology (Fridman and Shwageraus, 2013; Rachamin et al., 2013; Nikitin et al., 2015a, 2015b), the updating of the thermal-hydraulic (TH) database with thermal-physical properties of sodium, and the development of the thermal-mechanical (TM) model to account for thermal expansion effects of the core components.

Part I of the paper (Nikitin et al., 2018a) provided a detailed description of the thermal expansion models that have recently been implemented in DYN3D. The models enable the treatment of important thermal expansion effects occurring within the SFR core, in particular axial expansion of fuel rod and radial expansion of diagrid. The axial expansion model is capable of modeling non-uniform core expansions by using the spatial temperature distribution of the fuel rods. The radial diagrid expansion model utilizes the average inlet sodium temperature to uniformly expand the core in the radial direction. The initial verification study, summarized in Part I of the paper, demonstrated an adequate performance of the newly implemented models.

Part II of the paper focuses on the verification and validation of the extended version of DYN3D against the IAEA benchmark on the control rod (CR) withdrawal tests from the end-of-life (EOL) experiments conducted at the Phenix reactor (IAEA, 2014). The benchmark was designed to assess the capability of neutronic codes, used for SFR analyses, to model deformations in radial power distribution due to the various asymmetric arrangements of CRs. In order to take a full advantage of the available experimental data, the benchmark tasks were solved by DYN3D in two different ways: 1) neutronic solution without feedbacks, and 2) coupled solution with TH and TM feedbacks. The first one was obtained using the fixed core geometry while the dimensions of the fuel assemblies and other core components were explicitly expanded based on the average temperatures provided in the benchmark specifications. In contrast to the previous case, the second solution was obtained by invoking the thermal expansion models to obtain the actual core dimensions based on the temperatures provided by the TH module. In this study, the first solution is used to validate the few-group XS generation methodology and the neutronic performance of DYN3D in general, while the second one served to demonstrate and assess the overall capabilities of the extended DYN3D version.

The following section provides a brief overview of the CR withdrawal tests. The computational methodology and more detailed modeling assumptions are presented in Section 3. The numerical results obtained with the DYN3D are compared to the experimental data and other codes in Section 4. Section 5 summarizes the results of this part of the paper.

2. Description of the control rod withdrawal tests

The control rod withdrawal tests, documented in (IAEA, 2014), were part of the several EOL tests performed in 2009 at the Phenix reactor. The Phenix EOL core consists of 54 inner and 56 outer MOX fuel assemblies surrounded, first, by 86 blanket assemblies and, secondly, by 252 reflector assemblies on the periphery (see Fig. 1). Furthermore, the core comprises 6 primary CRs, one secondary CR, and 14 reflector-type assemblies inside the core and blanket region as depicted in Fig. 1.

During the control rod withdrawal tests, a series of steady-state measurement were conducted with four different CRs arrangements (hereafter referred to as the CR shift test). The main goal of the test was to investigate deformations of the radial power shape due to the asymmetric axial positioning of the shifted CRs. At the reference state, all six primary CRs were kept on equivalent level of elevation (so-called "rod bank" position). In three additional steps, CR #1 and #4 shown in Fig. 1 were either withdrawn or inserted relatively to the "rod bank" according to the sequence presented in Fig. 2. The rod bank position was adjusted to keep the reactor at constant power of about 335 MWth. The total sodium flow rate remained constant along all steps.

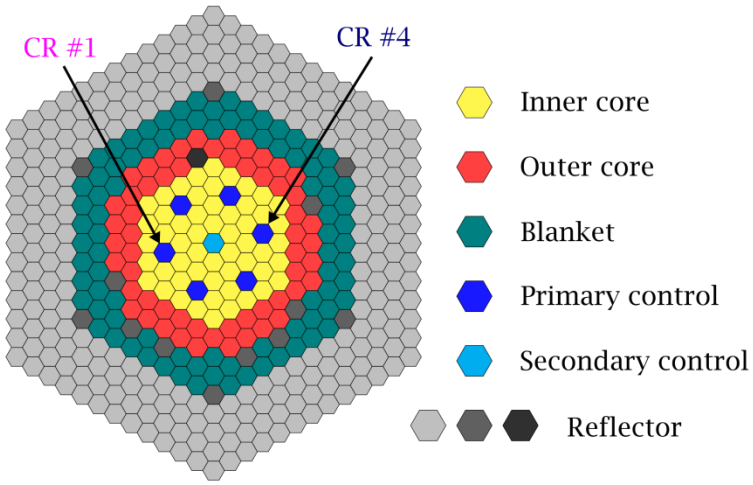

Fig. 1. Phenix EOL core: radial core layout and location of the shifted CRs.

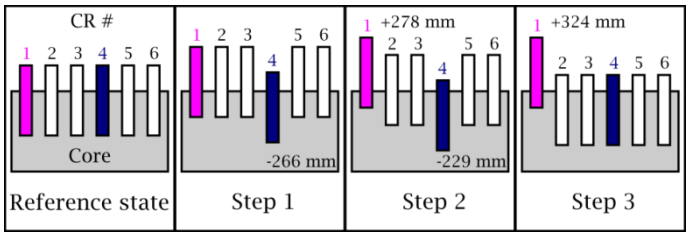

Fig. 2. CR shift sequence.

During the CR shift test, the sodium temperature was measured at the core outlet. Thermocouples were positioned at the head of each assembly located in the first seven assembly rows of the core starting from the

core center (120 thermocouples in total). Using these, the sodium heating (temperature difference between inlet and outlet) was measured assembly-wise at each step. The heat transfer between assemblies was assumed to be insignificant. Moreover, the change in the flowrate distribution due to the change of sodium heating was also assumed negligible. Based on these assumptions, the radial distribution of the relative power deviations in respect to the reference state was calculated for each step from the variation of sodium heating (IAEA, 2014):

$$\delta_{rel}P_i = \frac{P_i - P_i^{ref.}}{P_i^{ref.}} = \frac{Qc_P\left(\Delta T_i - \Delta T_i^{ref.}\right)}{Qc_P\Delta T_i^{ref.}} = \delta_{rel}(\Delta T_i), \quad (1)$$

where P is the assembly power, Q is the sodium mass flowrate, c_P is the assembly-average specific heat capacity, and ΔT is the sodium heating in the assembly i. The *ref.* index denotes the values taken from the reference state. In this study, the deviation in radial power distribution estimated from the temperature measurements for Steps 1-3 were used for the validation of the DYN3D code.

The reactivity worth of the two involved CRs was measured before the CR shift test. The balancing method was used to acquire the integral rod worth over the full range of withdrawal (S-curve) for the CR #1 and #4. The test was initiated at critical low power state (~50 kW), where CR #1 and CR #4 was in complete inserted and withdrawn position, respectively. By using a succession of elementary steps, the CR #4 was moved from bottom to top, while the CR #1 in the opposite direction. As presented in Fig. 3, the CR #4 was firstly moved downwards by a small increment (Step I in Fig. 3) and secondly the CR #1 was withdrawn to compensate the negative change of reactivity (Step II in Fig. 3). Between each elementary CR displacement, the differential worth was measured for each CR based on the application of the inverse kinetics method. When the CR #4 had been totally withdrawn to the top and CR #1 inserted to the bottom (Step N in Fig. 3), the full S-curves were obtained for both rods.

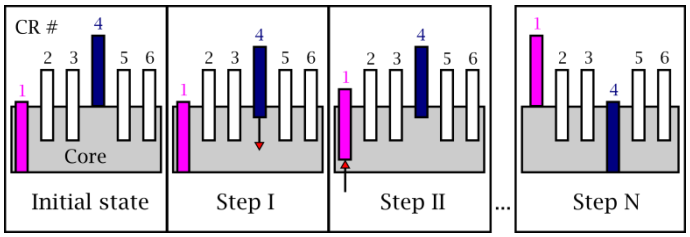

Fig. 3. Schematic representation of the balancing method.

3. Computational methodology

The calculations were done in a two-step approach using the Serpent-DYN3D codes sequence. In the first step, the homogenized few-group XS were generated on lattice level with Serpent, and in the second step, the full core nodal calculations were performed with DYN3D.

3.1 Generation of parametrized cross section libraries

A parametrized XS library was generated for DYN3D that covers the full range of reactor conditions of the CR withdrawal tests.

The XS were calculated with Serpent at different fuel temperatures, coolant temperatures, axial expansion and radial diagrid expansion states. Table 1 presents the selected states that span the parameter space of the XS library. In Table 1, the temperature-dependent expansion coefficients are defined as:

$$\varepsilon(T) = \frac{L(T)}{L(T_0)} = 1 + \alpha(T) \cdot (T - T_0), \tag{2}$$

where L is the linear dimension and α is the linear expansion coefficient corresponding to the temperature T, and T_0 is the reference temperature of the used linear expansion correlation. In this case, the correlation for the temperature-dependent linear expansion coefficients was provided in the benchmark specification.

Table 1. Conditions used for cross section parametrization.

Fuel temperature, K	Coolant temperature, K	Axial expansion	Radial expansion
523 900 1500 1800	523 900	$\varepsilon(523)$ $\varepsilon(1200)$	$\varepsilon(523)$ $\varepsilon(900)$

The coolant density variation is implicitly considered in the coolant temperature variation. In case of the axial expansion effect, the change of dimensions and densities is considered for both fuel and cladding. Furthermore, the radial expansion of the pins, the reduction in the liquid sodium amount between the pins, and the temperature effect of the cladding are taken into account. The axial expansion is assumed to be driven by the cladding temperature. When the diagrid is radially expanded, the assembly pitch size is increased (Fig. 4). At the same time, the dimensions of the pins and assembly wrapper remain unchanged, i.e. the increase of sodium gap between assemblies is modeled when the homogenized XS are generated.

The JEFF-3.1 based homogenized XS were obtained in the 24-group energy structure as suggested in (Fridman and Shwageraus, 2013). For further improvement of the nodal diffusion solution, the Superhomogenization (SPH) method (Kavenoky, 1978; Hebert, 1993) was applied for blanket and non-multiplying regions adjacent to the fuel nodes. The XS generation procedure for the Phenix core is presented in more details in Part I of the paper. The methodology to create Monte Carlo based homogenized XS for SFRs in general is discussed in the preceding papers by the authors (Nikitin et al., 2015a, 2015b).

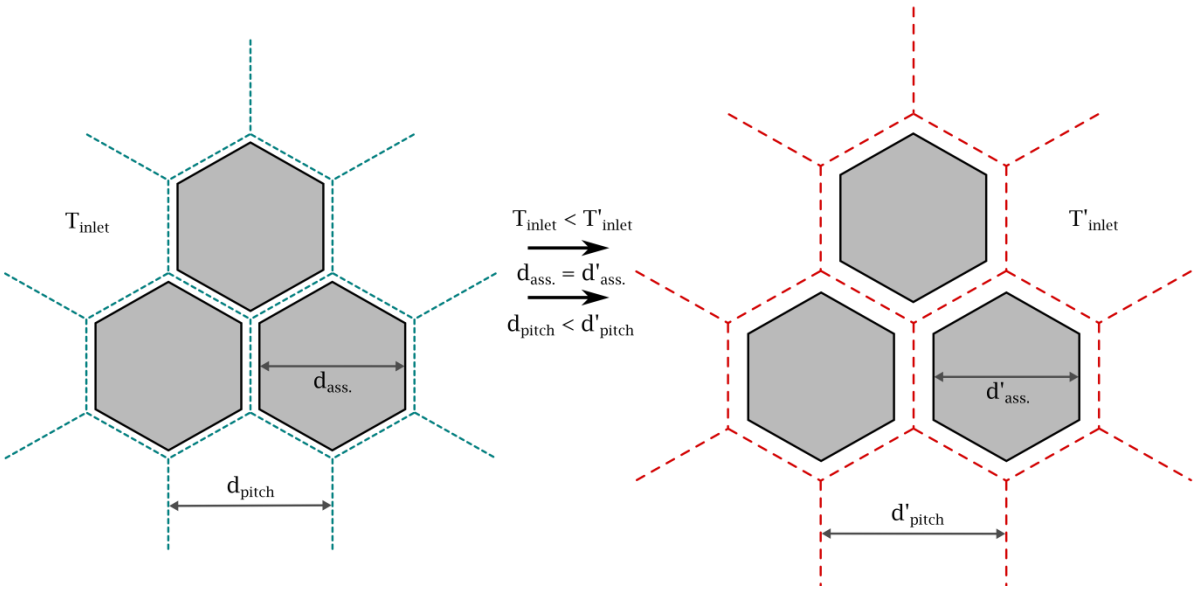

Fig. 4. Schematic overview of the radial core expansion.

3.2 DYN3D model

The Phenix EOL core model was constructed in DYN3D based on the data provided in the corresponding IAEA benchmark report. By using the homogenized XS generated with Serpent, the full core nodal diffusion solution was obtained with DYN3D for all four states of the test. The calculations were repeated in two different ways:

- Case A: Pure neutronic calculations employing the fixed uniform temperatures specified in the benchmark. This approach was adopted by the majority of the benchmark participants.
- Case B: Coupled neutronic thermal-hydraulic (N/TH) calculations employing the newly implemented axial fuel rod expansion model, where the axial expansion of the fuel rods was driven by local cladding temperatures.

Since Case A comprises only steady state neutronic calculations, the nodal mesh was expanded explicitly without applying the thermal expansion models. The following uniform temperatures were used in the CR shift test: 1500 K for the fuel, 900 K for the blanket, and 721 K for structural, coolant, and absorber materials. The latter temperature was used to uniformly expand the core in the axial direction. In the radial direction, the core was expanded according to the inlet temperature of 646 K.

In Cases B, the initial core dimensions were set according to the isothermal state of 250 °C. During calculations, the fuel rods were expanded using local cladding temperatures provided by the TH module of DYN3D. In order to ensure a more consistent comparison between the two cases, the gas gap conductance in the fuel rods was adjusted to reproduce the specified core-average fuel temperature of 1500 K. For all reactor states of the CR shift test, the total power and the boundary conditions (i.e. the inlet coolant temperature and the mass flow rate distribution) were set according to the benchmark specification.

The control rod S-curves of CR #1 and #4 were obtained with DYN3D by simulating the balancing method applied in the experiment (see Fig. 3). Since the core temperatures were not provided for this measurement, but the test was done in the low power state, it was assumed that the core resides in the isothermal condition (250 °C). The simulation comprises a succession of steady state calculations by using the approach of Case A, where all the temperatures were fixed at 250 °C. The DYN3D calculations were executed as follows:

1. The CR #1 and #4 were fixed in the totally inserted and withdrawn position, respectively. The rest of the CRs were moved together until critical state was achieved with DYN3D.
2. CR #4 was inserted further by one-ninth of full range of withdrawal, which corresponds to 100 mm at cold state (20 °C). This is equivalent to Step I in Fig. 3.
3. CR #1 was withdrawn further by one-ninth of full range of withdrawal. This corresponds to Step II in Fig. 3.
4. Step 2 and 3 were repeated with DYN3D until the final state was reached (Step N in Fig. 3).

The differential rod worth of each elementary displacement was obtained for both CRs. The S-curves were obtained by cumulative summation of the differential rod worths.

4. Numerical results

4.1 Case A - neutronic calculations

The DYN3D results were compared with the full core MC solution of Serpent and the measurements. The calculated core reactivity values are presented in The radial power distributions of all states calculated with Serpent are presented in Fig. 5 (top), and the comparison with DYN3D in Fig. 5 (bottom). The Serpent power distributions were obtained by the averaging the results of the 20 independent Serpent calculations each of which was executed with a total of 960 million active neutron histories (i.e. 1500 active and 200 skipped cycles with 640,000 neutron histories per cycle). As compared to Serpent, the power predicted with DYN3D does not exceed 1.5% for any state, while the average power deviation remains around 0.5%.

Table 2. In all steps, the codes noticeably overestimate the reactivity by about 430 to 600 pcm. Nevertheless, the Serpent and DYN3D results are very close and agree within about 160 pcm. Moreover, the reactivity swings between the steps remain below 15 pcm for both codes. The Serpent and DYN3D results are consistent with the results of the benchmark participants (IAEA, 2014, pp. 175–176) that presented a reactivity bias of around +730 pcm compared to the critical state. Such discrepancies do not only come from nuclear data and measurement uncertainties, but from the averaged description of the reactor core.

The radial power distributions of all states calculated with Serpent are presented in Fig. 5 (top), and the comparison with DYN3D in Fig. 5 (bottom). The Serpent power distributions were obtained by the averaging the results of the 20 independent Serpent calculations each of which was executed with a total of

960 million active neutron histories (i.e. 1500 active and 200 skipped cycles with 640,000 neutron histories per cycle). As compared to Serpent, the power predicted with DYN3D does not exceed 1.5% for any state, while the average power deviation remains around 0.5%.

Table 2. Calculated core reactivity at all states.

(pcm)	Case A			Case B
	Serpent	DYN3D	Serpent vs. DYN3D	DYN3D
Ref. state	584 ± 2	421	-162	463
Step 1	592 ± 2	436	-157	436
Step 2	596 ± 2	436	-161	455
Step 3	596 ± 2	432	-165	474

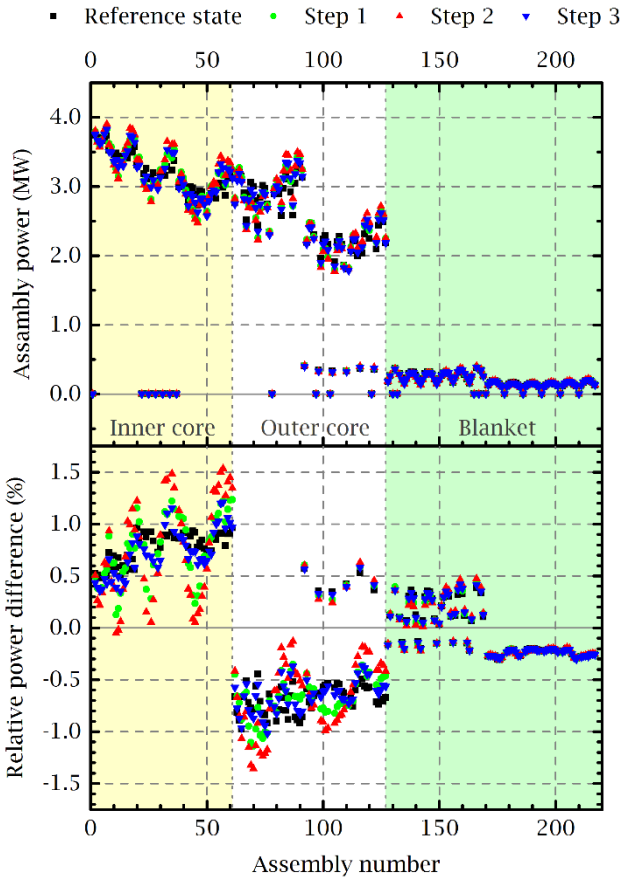

Fig. 5. Radial power distribution calculated with Serpent for all states (*top*), and the relative difference in power between DYN3D and Serpent (*bottom*).

The power deviation profiles obtained with Eq. (1) from the DYN3D solutions are presented in Fig. 6a. The maximal positive and negative power deviations of all steps are compared against the Serpent results and the experiment in Table 3. It is clearly seen that the maximal distortion of the power shape is achieved when the CRs #1 and #4 are shifted in opposite directions (i.e. at Step 2). In this step, according to the

experimental data, the power is increased by 12.1% and reduced by 10.9% around the extracted and inserted CRs, respectively. At Step 1 and 3, when only one CR is shifted relatively to the bank, a compensation effect can be observed on the opposite side of the involved CR which is caused by keeping the core on constant power (Pascal et al., 2013).

As compared to the experimental data, the codes consistently overestimate the effect of the CR shift and predict considerably higher limits in the assembly-wise power deviation distributions (Table 3). Nevertheless, a very good agreement is observed between the MC and nodal diffusion methods. The discrepancy in power deviations does not exceed 0.5%, even in the second step, as demonstrated in Fig. 6b. The average difference between the codes is ±0.1 / 0.2 / 0.1% for step 1, 2, and 3 respectively.

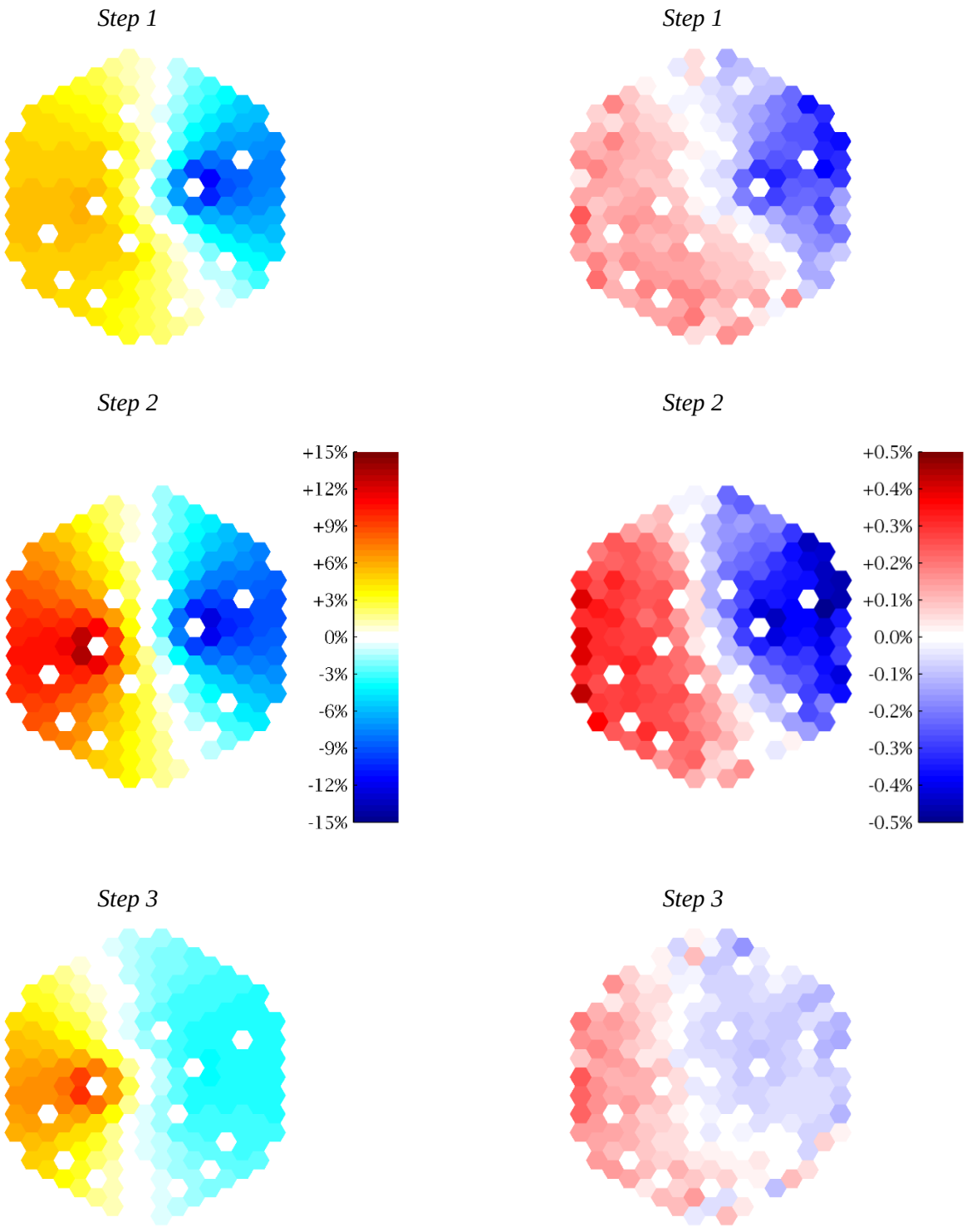

a) Power deviations calculated with DYN3D *b) Difference in power deviations, DYN3D vs. Serpent*

Fig. 6. Radial distribution of the power deviations for all steps (a), and the difference between DYN3D and Serpent results (b).

Table 3. Comparison of maximal power deviations at all steps.

(%)	Step 1			Step 2			Step 3		
	Exp.	Serpent	DYN3D	Exp.	Serpent	DYN3D	Exp.	Serpent	DYN3D
Max. positive deviation	N.A.	5.8	6.0	12.1 ± 1.4	13.0	13.3	9.1 ± 1.4	9.5	9.6
Max. negative deviation	-9.5 ± 1.3	-11.2	-11.5	-10.9 ± 1.3	-12.4	-12.8	N.A.	-3.9	-4.0

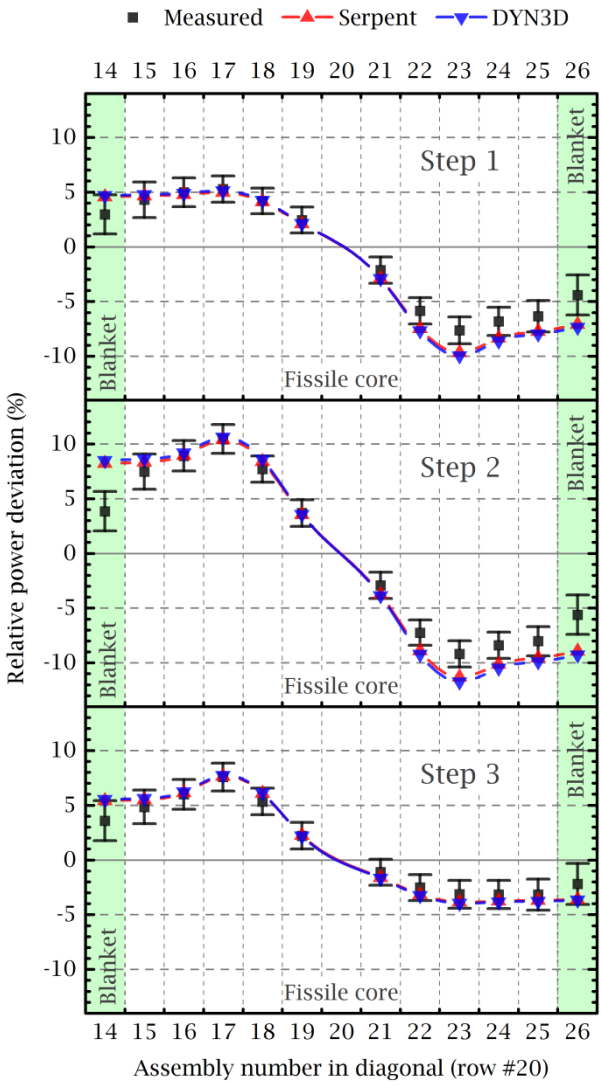

Fig. 7. Comparison of radial deviation profiles along the diagonal closest to CRs #1 and #4 (*Top* to *bottom*: Step 1 to Step 3). DYN3D results are from Case A.

The calculated power deviations, extracted from the core diagonal closest to CR #1 and #4, were compared with each other and the measurements in Fig. 7. The power deviation profiles predicted by DYN3D are in a very good agreement with MC solutions while the maximal differences in the order of the steps are about 0.3%, 0.4% and 0.1%. While the computational results remain within the experimental uncertainty band at the center of the core and around the withdrawn CR, higher discrepancies are observed

in the blanket assemblies and around the inserted CR (Fig. 7). The highest deviation between DYN3D and the measurement occurs at Step 2, where the maximal differences are around 2.6% and 4.7% in the fissile core and blanket, respectively. Although the discrepancies between DYN3D and the measurement are significant, the DYN3D solution remains within the range of results provided by all other benchmark participants (IAEA, 2014, pp. 209–211).

In general, all codes applied in the benchmark overestimate the power deviations. The discrepancies observed between the experiment and the computational results presented in this paper and the benchmark report are mainly caused by measurements problems explained by (Pascal et al., 2013). Some of the TH effects were disregarded that lead to an overestimation in the peripheral assemblies. The neglected phenomena were the heat transfer between the fertile and fissile assemblies, and the turbulent mixing between the sodium streams of these assemblies and the hot plenum. Still, the systematic overestimation along the whole core is mainly associated with uncertainties of the provided CR positions. These were obtained during the test with the help of empirical models that considered the relative thermal expansions of the core, vessel and CRs.

Additionally to the CR shift test, the balancing method was simulated with DYN3D and Serpent to obtain the S-curves for CR #1 and #4. The Serpent simulation followed the same procedure as described for DYN3D in Section 3.2. The statistical uncertainty of the Serpent reactivities was kept under 2 pcm. The calculated and measured (IAEA, 2014, p. 18) S-curves of both CRs are compared in Fig. 8. The total rod worths are summarized in Table 4. The DYN3D overestimates both the Serpent rod worths by 66 and 53 pcm and the measured ones by 75 and 24 pcm for CR #1 and #4, respectively. Nevertheless, the computational results are in a very good agreement with the experimental data while the S-curves are well aligned with each other.

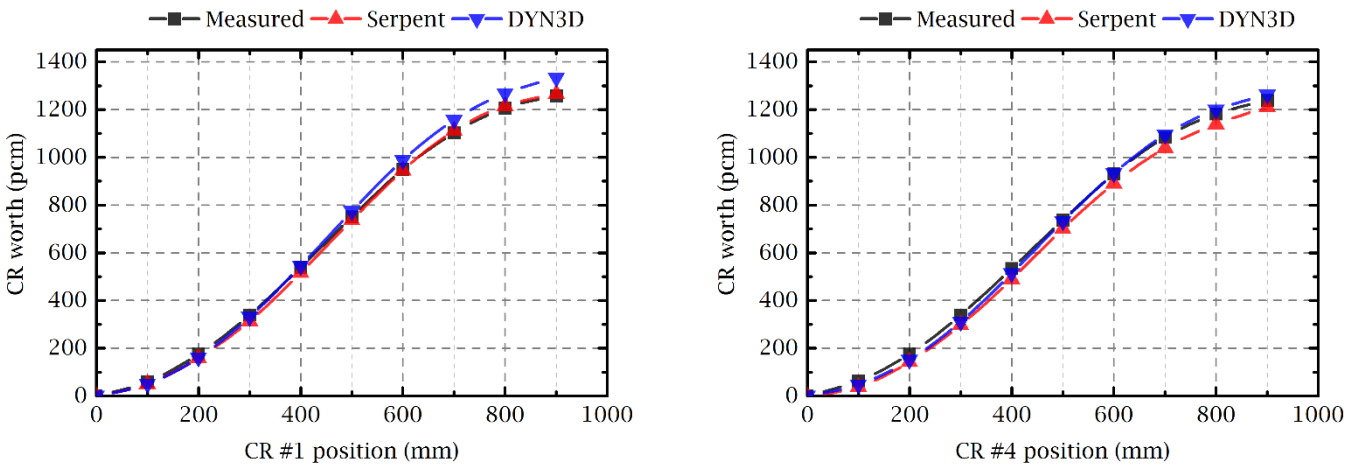

a) CR #1 *b) CR #4*

Fig. 8. Comparison of control rod S-curves.

Table 4. Measured and calculated control rod worths for CR #1 and #4.

(pcm)	DYN3D	Serpent	Experiment	DYN3D vs. Serpent	DYN3D vs. Experiment
CR #1	1332	1266	1257	66	75
CR #4	1262	1209	1238	53	24

4.2 Case B - Coupled neutronic thermal-hydraulic calculations

Beside the Case A results, The radial power distributions of all states calculated with Serpent are presented in Fig. 5 (top), and the comparison with DYN3D in Fig. 5 (bottom). The Serpent power distributions were obtained by the averaging the results of the 20 independent Serpent calculations each of which was executed with a total of 960 million active neutron histories (i.e. 1500 active and 200 skipped cycles with 640,000 neutron histories per cycle). As compared to Serpent, the power predicted with DYN3D does not exceed 1.5% for any state, while the average power deviation remains around 0.5%.

Table 2 also contains the reactivity values obtained with DYN3D in the coupled neutronic thermal-hydraulic calculation mode. For Case B, the reactivity remains overestimated by around 430-470 pcm.

The impact of using coupled N/TH analysis instead of the pure neutronic calculation with uniform temperature profiles was assessed by comparing the obtained radial power deviation profiles against the measured ones. Fig. 9 presents the discrepancies between DYN3D and the experiment for all steps obtained as:

$$\Delta(\delta_{rel}P)_i = \delta_{rel}P_i^C - \delta_{rel}P_i^E, \quad (4)$$

where $\delta_{rel}P$ is the relative power deviation obtained with Eq. (1) for each assembly *i* from the experiment (*E*) and DYN3D calculations (*C*). The results of the coupled calculations (Case B) are almost aligned with the pure neutronic solution (Case A), but a slight reduction of discrepancies is observed in Case B (Fig. 9).

In Case B, a more realistic expansion of each fuel assembly was modelled with DYN3D by using the cladding temperature distribution. Fig. 10 presents axial expansion profile of the diagonal assemblies calculated for Step 2 with DYN3D. The profile is obtained as the difference in height between the expanded and reference state (20 °C):

$$\Delta L = L_{exp} - L_{ref}. \quad (5)$$

The expansion profile reveals that, while the central assemblies become larger, the assemblies on the periphery remain smaller than in case of uniform expansion. Furthermore, Fig. 10 shows that the expansion of an assembly is following the axial sodium heat-up, i.e. the upper nodes expand more than the lower ones. DYN3D uses these self-calculated node-wise expansion profiles to obtain the correct XS with the mixing approach as described in details in Part I of this paper.

As compared to the experiment in general, the results demonstrated a competent performance of the coupled code. Although the more realistic expansion profile obtained from the new TM model did not affect

the steady state results notably, the application of this new model can be important in transient and accident analyses where the significantly higher temperature variations can be expected.

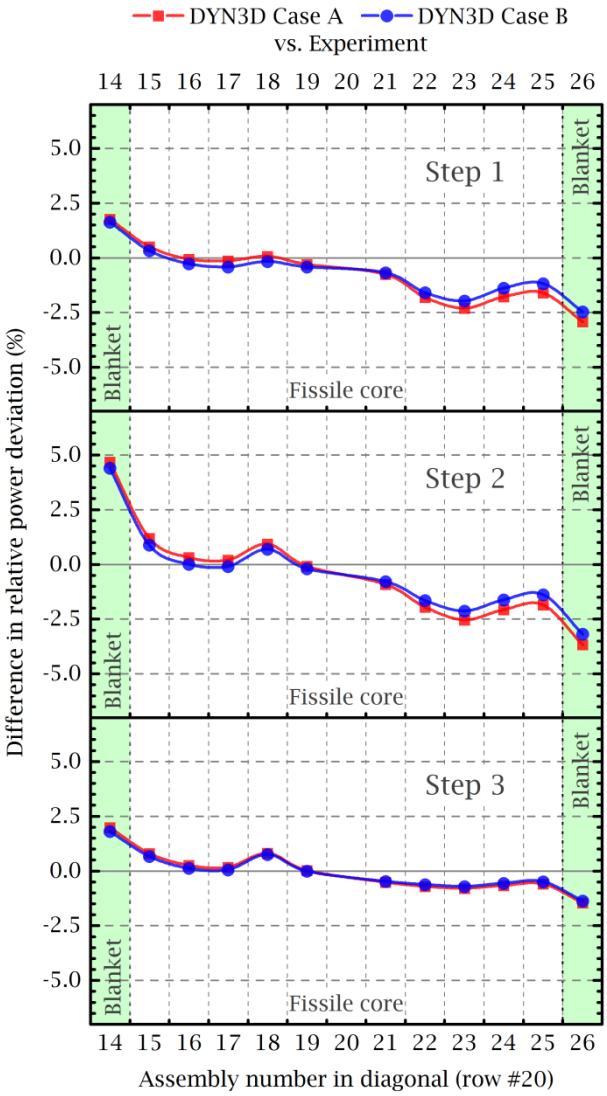

Fig. 9. Difference in power deviation profiles between DYN3D and the experiment (*Top* to *bottom*: Step 1 to Step 3). The results are depicted along the diagonal closest to CRs #1 and #4.

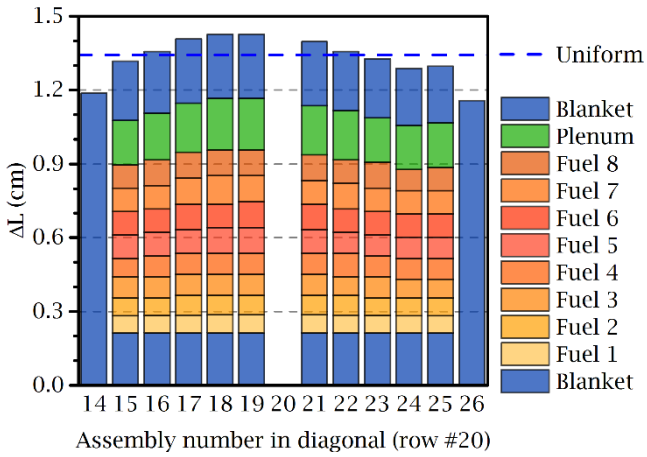

Fig. 10. Absolute axial expansion profile of assemblies along the diagonal closest to CRs #1 and #4. Calculated with DYN3D.

5. Summary of the results

This paper presented the verification and validation of the extended version of DYN3D against the Phenix EOL control rod withdrawal benchmark. The benchmark tasks were solved by DYN3D in two different ways: 1) pure neutronic calculations without feedbacks, and 2) coupled N/TH calculations with consideration of local thermal expansion effects. In both cases the homogenized XS were generated with Serpent. The obtained DYN3D results are summarized as follows:

- By using the first method the CR shift test and the CR S-curve measurements were modeled with DYN3D. These solutions were used to validate the few-group XS generation methodology and neutronic performance of DYN3D in general:
  - The DYN3D results are in very good agreement with the full core MC solution of Serpent and they are consistent with the numerical solutions of the benchmark participants.
  - Similarly to the benchmark participants, significant discrepancies were observed between the DYN3D solutions and the experimental data. These were explained with the aforementioned benchmark deficiencies, e.g., the averaged core descriptions and the uncertainties of the provided CR positions.
  - The integral CR worths and the S-curves are in good agreement with the Serpent solution as well as with the experimental data.
- In the second case, only the CR shift test was modeled to demonstrate and assess the overall capabilities of the extended DYN3D version:
  - The coupled N/TH calculations presented an adequate performance, while predicting realistic thermal expansion profiles of the fuel assemblies. The results were not significantly different from the solution where the core-average temperature was used to uniformly expand the core.

– It is worth noting that in more severe cases, when the local temperature variations are higher, the selection between uniform and non-uniform axial thermal expansion modeling can be more influential on the results.

In the subsequent Part III of the paper (Nikitin et al., 2018b), the extended DYN3D is assessed for transient analyses by validation against the initial stage of then Phenix EOL natural convection test (IAEA, 2013). This transient case is in particular importance, since the DYN3D has to properly account for the dynamic behavior of the axial and radial core dimensions.

Acknowledgements

The work carried out by HZDR was partly supported by a project of the German Federal Ministry for Economic Affairs and Energy (BMWi) (registration number 150 1462).

References

Fridman, E., Shwageraus, E., 2013. Modeling of SFR cores with Serpent-DYN3D codes sequence. Annals of Nuclear Energy 53, pp. 354–363.

Hebert, A., 1993. Consistent technique for the pin-by-pin homogenization of a pressurized water reactor assembly. Nuclear Science and Engineering 113, pp. 227–238.

IAEA, 2014. Benchmark Analyses on the Control Rod Withdrawal Tests Performed during the PHENIX End-of-Life Experiments, IAEA-TECDOC-1742, International Atomic Energy Agency, Vienna, Austria.

IAEA, 2013. Benchmark Analyses on the Natural Circulation Test Performed During the PHENIX End-of-Life Experiments, IAEA-TECDOC-1703, International Atomic Energy Agency, Vienna, Austria.

Kavenoky, A., 1978. The SPH Homogenization Method, in Proc.: A Specialists' Meeting on Homogenization Methods in Reactor Physics, IAEA-TECDOC-231, Lugano, Switzerland.

Nikitin, E., Fridman, E., Mikityuk, K., 2015a. Solution of the OECD/NEA neutronic SFR benchmark with Serpent-DYN3D and Serpent-PARCS code systems. Annals of Nuclear Energy 75, pp. 492–497.

Nikitin, E., Fridman, E., Mikityuk, K., 2015b. On the use of the SPH method in nodal diffusion analyses of SFR cores. Annals of Nuclear Energy 85, pp. 544–551.

Nikitin, E., Fridman, E., Pautz, A., 2018a. Extension of the reactor dynamics code DYN3D for SFR applications – Part I: thermal expansion models. Annals of Nuclear Energy, submitted.

Nikitin, E., Fridman, E., Pautz, A., 2018b. Extension of the reactor dynamics code DYN3D for SFR applications – Part III: validation against the initial phase of the Phenix EOL natural convection test. Annals of Nuclear Energy, submitted.

Pascal, V., Prulhière, G., Vanier, M., Fontaine, B., 2013. Interpretation of the Control Rod Withdrawal Test in the Sodium-Cooled Fast Reactor Phénix. Nuclear Science and Engineering 175, pp. 109–123.

Rachamin, R., Wemple, C., Fridman, E., 2013. Neutronic analysis of SFR core with HELIOS-2, Serpent, and DYN3D codes. Annals of Nuclear Energy 55, pp. 194–204.

Rohde, U., Kliem, S., Grundmann, U., Baier, S., Bilodid, Y., Duerigen, S., Fridman, E., Gommlich, A., Grahn, A., Holt, L., Kozmenkov, Y., Mittag, S., 2016. The reactor dynamics code DYN3D – models, validation and applications. Progress in Nuclear Energy 89, pp. 170–190.